Probing Pb + Pb collisions at $\sqrt{S_{NN}} = 2760$ GeV with spectators

Vipul Bairathi [a], Sandeep Chatterjee [b,*], Md. Rihan Haque [a], Bedangadas Mohanty [a]

[a] *School of Physical Sciences, National Institute of Science Education and Research, Jatni, 752050, India*
[b] *Theoretical Physics Division, Variable Energy Cyclotron Centre, 1/AF Bidhannagar, Kolkata, 700064, India*

ARTICLE INFO

ABSTRACT

There is event by event geometric as well as quantum fluctuations in the initial condition of heavy-ion collisions. The standard technique of analysing heavy-ion collisions in bins of centrality obtained from final state multiplicity averages out the various initial configurations and thus restricts the study to only a limited range of initial conditions. In this paper, we propose an additional binning in terms of total spectator neutrons in an event. This offers us a key control parameter to probe events with broader range of initial conditions providing us an opportunity to peep into events with rarer initial conditions which otherwise get masked when analysed by centrality binning alone. We find that the inclusion of spectator binning allows one to vary ε_2 and ε_3 independently. We observe that the standard scaling relation between v_2/ε_2 and $\frac{1}{S}\frac{dN_{ch}}{d\eta}$ exhibited by centrality bins is strongly broken by the spectator neutron bins. Further, the acoustic scaling relation between $\ln(v_n/\varepsilon_n)$ and transverse system size is also broken- the strength of the breaking being sensitive to the binning procedure. The introduction of the spectator binning allows us to tune over a wide range viscosity driven effects for events with varying initial states but similar final state multiplicity.

1. Introduction

Of all the stages in a heavy-ion collision (HIC), the initial stage is the least understood. However, in order to perform a sensitive test of the theoretical framework, e.g. relativistic viscous hydrodynamics, that correctly describes the evolution of the strongly interacting matter produced in HIC experiments and thereof allows unambiguous extraction of the medium properties, e.g. values of the transport coefficients, require a precise knowledge of the initial state (IS). It has been shown that depending on the choice of the initial condition that one chooses to evolve the relativistic hydrodynamic equations, the value of the extracted shear viscosity to entropy density ratio at the RHIC 200 GeV can vary by a factor of 2 [1–6].

The nuclei used in HIC experiments are extended objects. This results in event by event (E/E) geometrical fluctuations in addition to the intrinsic quantum fluctuations of the nuclear wave function. The geometry of the nucleus ensures that various characteristics of the IS in HICs like the number of wounded nucleons N_{part}, number of binary collisions N_{coll}, shape of the overlap region, say the ellipticity ε_2, are all correlated with the impact parameter b. However, none of the above IS collision attributes is directly observed in experiments. This makes the job to constrain the IS very challenging. The standard method uses the final state (FS) charged particle multiplicity to characterise the events into different centrality classes corresponding to different ISs. However, the geometric and quantum E/E fluctuations in the IS result in appreciable variation of b, N_{part}, N_{coll}, ε_2 etc., even within the same centrality bin. Thus, a lack of proper knowledge of the IS is a major hindrance towards carrying out precise comparisons between theory and experiments. In this work, we focus on the spectators (those nucleons which do not participate in the collision) and show that it is possible to extract vital information of the IS by analysing them. The significant role played by spectator asymmetry in the various experimental observables and the possibility of selecting special initial configurations in HIC using deformed U nuclei has been pointed out recently [7,8]. In a study based on Monte Carlo Glauber model simulations it was suggested that spectator asymmetry could be used to trigger specific collision configurations called Body-Tip with sufficient magnetic field and much lower ellipticity which can lead to the disentanglement of chiral magnetic effect from its dominant background anisotropic flow in $U + U$ collisions [7]. In Ref. [8] it was demonstrated based on A Multi Phase Trasport (AMPT) model simulations that spectator asymmetry could be utilised to identify

* Corresponding author.
E-mail addresses: vipul.bairathi@niser.ac.in (V. Bairathi), sandeepc@vecc.gov.in (S. Chatterjee), rihan.h@niser.ac.in (Md. Rihan Haque), bedanga@niser.ac.in (B. Mohanty).
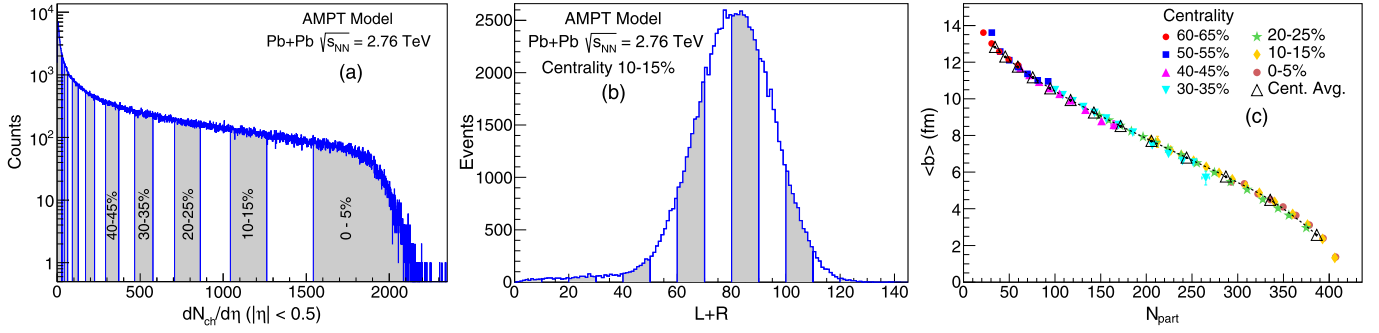
Fig. 1. (Colour online.) Left: The multiplicity distribution for min bias Pb–Pb events at $\sqrt{s_{NN}} = 2760$ GeV. In alternate white and grey bands, different centrality bins are also shown. Middle: The total spectator neutron number $L + R$ distribution for the $(10–15)\%$ centrality. The different $L + R$ bins are also shown. Right: The impact parameter b for the different centrality and $L + R$ bins are shown.

Body-Tip collision configurations in $U + U$ with large forward–backward asymmetry in particle production as well as considerably smaller elliptic flow, v_2. In this work, we look into the possibility of probing HICs of non-deformed nuclei using spectators. We will in particular focus on Pb + Pb collisions at $\sqrt{s_{NN}} = 2760$ GeV. A recent study has pointed out the correlation between forward–backward asymmetry in particle production and spectator asymmetry in Pb + Pb collisions at $\sqrt{s_{NN}} = 2760$ GeV [9].

We have constructed an IS observable, namely the total spectator neutron ($L+R$), which is the sum of the left going (L) and right going (R) spectator neutrons that are detected by the zero degree calorimeters (ZDC). The spectator protons never reach the ZDC as they are bent by the magnetic field and hit the beam pipe wall in experiments say for example at RHIC. Hence we do not consider them. With the present design of the ZDC, faithful measurements of spectator neutrons are limited to central and mid-central collisions upto ∼40% centrality due to clustering effects [10]. However, there are suggestions for advanced designs with much improved ZDC performance which could be implemented in the future [11]. In the absence of the IS fluctuations, $L + R$ and b would have a one to one correspondence. Both quantities are zero for full overlap collisions and increase for peripheral collisions. The advantage of $L + R$ is that it is an observable measured in experiments while b is never measured. We demonstrate that by performing a further binning over $L + R$ in addition to the standard centrality binning, it is possible to probe the fireball with novel IS conditions as compared to centrality binning alone. This allows us to perform a more accurate comparison between model predictions and data, thus enabling a more precise modelling and comprehensive understanding of the response of the strongly interacting matter to the IS conditions created in HIC experiments. The outline of the paper is as follows: in the section 2 we discuss the details of the AMPT model and our simulation as well as our proposed methodology to bin events. In Sec. 3, we show the main results obtained with this new binning procedure and finally summarise in Sec. 4.

2. Model

We have simulated Pb + Pb collisions at $\sqrt{s_{NN}} = 2760$ GeV using A Multi Phase Transport (AMPT) [12,13] model in the Default version. The AMPT model uses the same initial conditions as HIJING [14]. Zhangs parton cascade follows to take into account partonic interactions [15] which finally recombine with their parent strings that fragment into hadrons within the Lund String Fragmentation model [16]. There is a final stage hadronic afterburner before the hadrons freezeout. In this study we have analysed ∼2 × 10^6 events.

The standard practice is to first categorise events into different centrality classes according to charged particle multiplicity. This is

shown in Fig. 1(a). The different centrality classes are shown in alternate white and grey bands. Here we propose to do a second round of binning with the observable $L + R$ within each centrality bin. The $L + R$ binning is illustrated in Fig. 1(b) where the $L + R$ distribution is shown for $(10–15)\%$ centrality. The $L + R$ distribution shows a prominent peak around 85–95 and falls off rapidly on either side – the number of events drop by a factor of 5 as $L + R$ shifts by ∼20. Thus when the analysis is performed based on centrality binning alone, we mainly study properties of the events with total spectator neutrons around 85–95. Here with the introduction of the $L + R$ binning, we can investigate properties of the rare events with fewer or higher values of $L + R$ compared to the centrality mean value. This is the basic reason why additional $L + R$ binning on top of the centrality binning allows us to study new IS conditions in HICs. In Fig. 1(c) we have shown the variation of b with N_{part}. We find the centrality and $L + R$ bins to follow the same trend. However as shown in Figs. 2, 3 and 4, other IS attributes show different trends along centrality and $L + R$ bins that finally translate into different FS observable trends.

3. Results and discussion

We will now present the results of our analysis based on the spectator binning on top of the multiplicity binning. We show the results from centrality binning alone by the open triangles joined by a dotted line. Here we propose to further bin each such centrality bin into different $L + R$ spectator bins as well. These are shown by the coloured symbols, each colour representing a centrality bin.

Due to E/E fluctuation of the participant positions, the principal axes of inertia of the participant (P) nucleons is shifted as well as tilted with respect to those of the nucleus–nucleus (N) system [17]. Hence, we first perform the necessary translation,

$$x' = x_N - \langle x_N \rangle, \tag{1}$$

$$y' = y_N - \langle y_N \rangle, \tag{2}$$

where (x_N, y_N) denote the nucleon coordinates in the N coordinate system, and further rotate the primed coordinate system by the second order participant plane angle Ψ_2^{PP}, so as to coincide with the P coordinate system. Ψ_2^{PP} is obtained as follows,

$$\varepsilon_n e^{in\Psi_n^{\text{PP}}} = \frac{\sum_i r_i'^n e^{in\phi_i'}}{\sum_i r_i'^n}, \tag{3}$$

where (r_i', ϕ_i') is the new 2-D polar coordinate of the ith participant in the primed coordinate system. Ψ_2^{PP} is obtained for $n = 2$. The initial spatial geometry of the overlap region is encoded in the eccentricities ε_n defined in Eq. (3) of which ε_2 and ε_3 will be discussed in this work.
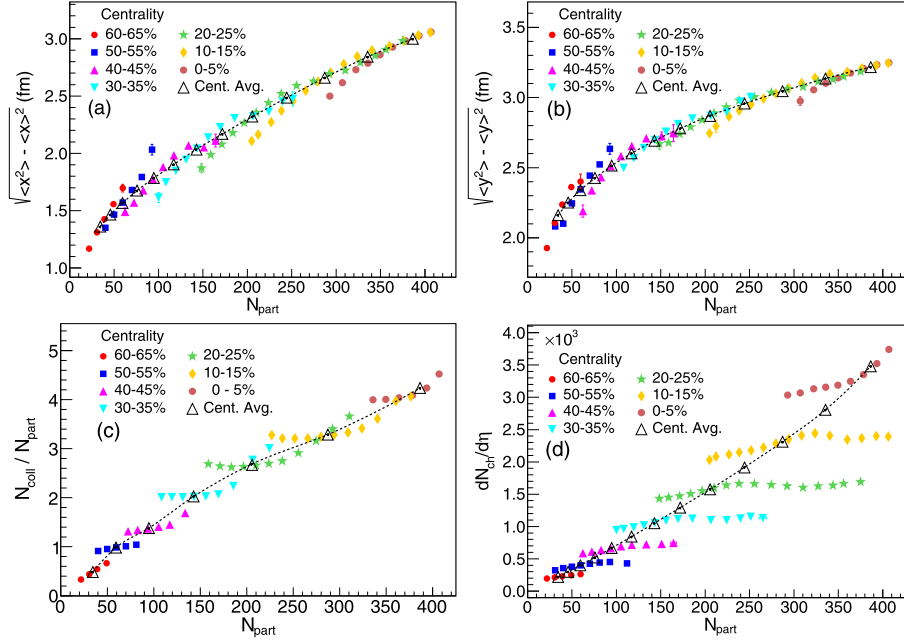
Fig. 2. (Colour online.) Different qualitative dependence of σ_x, σ_y, N_{coll} and $dN_{ch}/d\eta$ on N_{part} with centrality bins and $L+R$ bins.

We will first analyse the distribution of the participants in the plane transverse to the collision axis, which we call the collision plane. In Figs. 2(a) and 2(b) we have plotted the bin average of the standard deviation in the x_P ($\sigma_x = \sqrt{\langle x_P^2 \rangle - \langle x_P \rangle^2}$) and y_P ($\sigma_y = \sqrt{\langle y_P^2 \rangle - \langle y_P \rangle^2}$) coordinates of the participants measured with respect to the P coordinate system. σ_x and σ_y gives us an idea of the initial size of the fireball on the collision plane at the time of collision. The curves for σ_x and σ_y vs N_{part} show different correlations along centrality and $L+R$ bins. They both decrease more rapidly along $L+R$ bins than along centrality bins. This brings us to Fig. 2(c) where the number of binary collisions, N_{coll} is shown normalised to N_{part}, the number of participants. Within a geometry based approach of particle production and initial conditions in HICs, e.g. the two component Glauber model, N_{part} and N_{coll} are the two most essential ingredients that determine the IS as well as the FS multiplicity [18–20]. A collision between two nucleons (one from each of the colliding nucleus A and B) with coordinates (x_A, y_A) and (x_B, y_B) on the collision plane occurs if they satisfy the following simple geometrical criteria

$$(x_A - x_B)^2 + (y_A - y_B)^2 \leq \frac{\sigma_{NN}}{\pi} \qquad (4)$$

where σ_{NN} is the nucleon–nucleon cross section. N_{part} is the sum of all the nucleons that satisfy Eq. (4). N_{coll}, on the other hand, is the sum of all such possible binary collisions between the participants. The distribution of the participants on the collision plane determine the IS eccentricities given by Eq. (3). As shown in Fig. 2(c), the $L+R$ bins of a higher centrality bin mostly have larger value of N_{coll} compared to a lower centrality bin. This is so because as seen in Figs. 2(a) and (b), bins with same N_{part} but higher centrality occupy a smaller area on the collision plane as implied by smaller values of σ_x and σ_y. This means the participants are more lined up along the beam axis than perpendicular to it, hence having a higher value for N_{coll} and smaller σ_x and σ_y. Finally in Fig. 2(d) we have plotted $dN_{ch}/d\eta$ vs N_{part}. Clearly, the correlations along centrality bins is different from that along the $L+R$ bins. In a given centrality bin as $L+R$ increases, N_{part} decreases. However, $dN_{ch}/d\eta$ almost remains constant which in turn

implies constancy of the initial energy deposited even though N_{part} decreases. This suggests that in a given centrality, as we go towards bins with larger $L+R$, the energy deposit pattern changes-one expects to find larger energy gradients and more number of energy hot spots (as the same energy is deposited over a smaller transverse area by lesser N_{part}). This should result in very different viscous effects as one scans over bins with varying $L+R$ at a given centrality which will be best borne out by observables on anisotropic flow.

The collective hydrodynamic response converts the IS spatial anisotropy of the fireball as reflected by ε_n into the FS azimuthal anisotropy of the produced charged particle characterised by the flow observables $\left(v_n, \Psi_n^{EP}\right)$,

$$\frac{dN}{d\phi} \propto 1 + 2\sum_{n=1}^{\infty} v_n \cos\left(n\left(\phi - \Psi_n^{EP}\right)\right)$$

$$= 1 + 2\sum_{n=1}^{\infty} \left(v_{n,x}\cos(n\phi) + v_{n,y}\sin(n\phi)\right), \qquad (5)$$

$$Q_{n,x} = \sum_{i}^{M} \cos(n\phi_i), \qquad Q_{n,y} = \sum_{i}^{M} \sin(n\phi_i), \qquad (6)$$

$$v_{n,x} = \frac{1}{M}Q_{n,x}, \qquad v_{n,y} = \frac{1}{M}Q_{n,y}, \qquad v_n = \sqrt{v_{n,x}^2 + v_{n,y}^2} \qquad (7)$$

Here ϕ_i is the azimuthal angle of the ith particle, M is the total number of particles and Ψ_n^{EP} is the event plane angle, measured using the produced particles [21]. There have been attempts to study the influence of the initial event shape on the ensuing fireball dynamics and hence on various FS observables [22,23]. We now focus our attention on the event shape- how $L+R$ binning introduces a control parameter to tune the IS geometry.

From Figs. 3(a) and (c) it is clear that ε_2 and ε_3 can be tuned by simply triggering on different $L+R$ bins within a particular centrality bin. Thus the spectator bins allow a direct access to the initial event shape. ε_2 and ε_3 show almost similar variation along centrality and spectator bins for central events. For mid-central to peripheral bins, starting from (20–25)% centrality bin, the correlation between ε_2 and N_{part} along spectator bins is slightly steeper
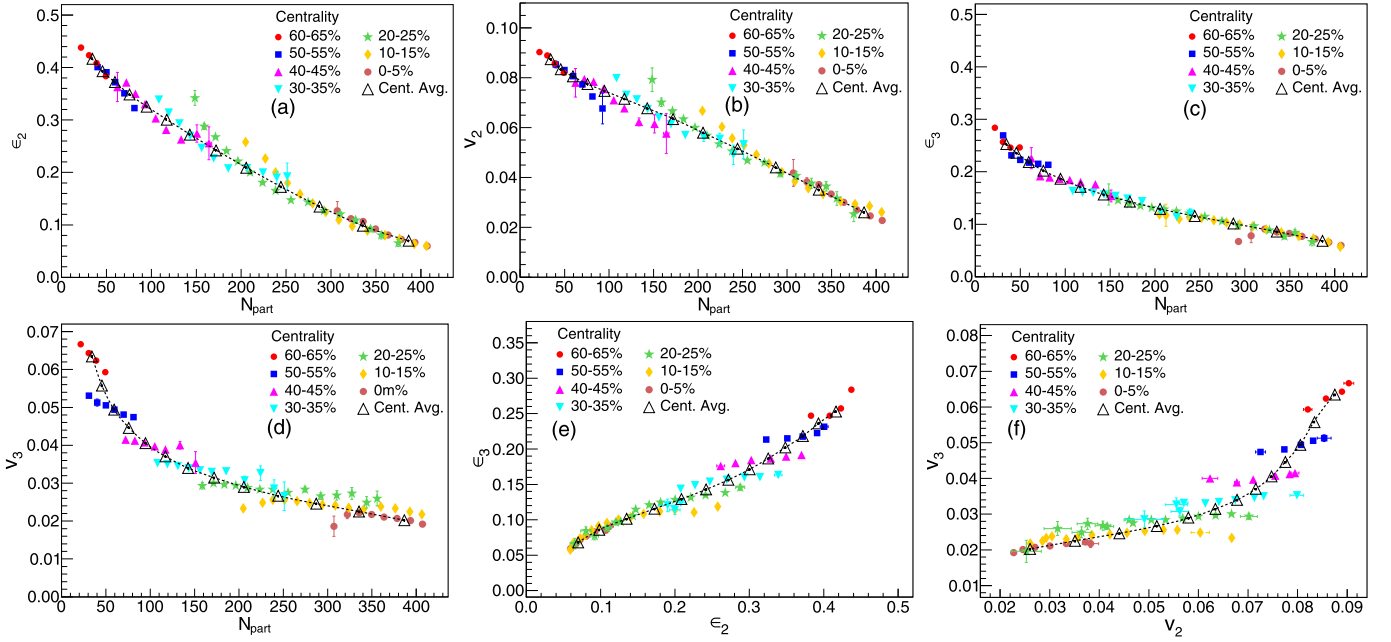
Fig. 3. (Colour online.) Different qualitative dependence of ε_2, ε_3, v_2 and v_3 on N_{part} with centrality bins and $L+R$ bins are shown. We also show the correlation between ε_2 and ε_3 as well as between v_2 and v_3 with centrality and $L+R$ bins.
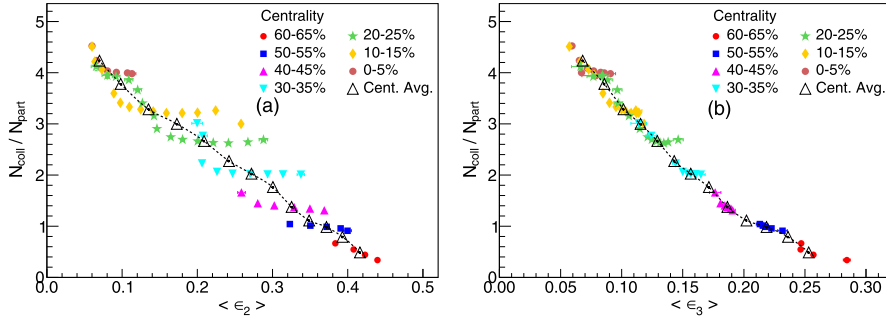

Fig. 4. (Colour online.) The correlation between $\varepsilon_2 - N_{\mathrm{coll}}/N_{\mathrm{part}}$ and $\varepsilon_3 - N_{\mathrm{coll}}/N_{\mathrm{part}}$ for different centrality and $L+R$ bins.

compared to that along centrality bins. On the other hand, ε_3 correlation with N_{part} is gentler along $L+R$ bins. This difference in variation of ε_2 and ε_3 along $L+R$ vs centrality bins becomes more transparent in the FS flow observables, v_2 and v_3 as shown in Figs. 3(b) and (d). We note that the $L+R$ bins preserve the usual linear relation between $(\varepsilon_2, \varepsilon_3)$ and (v_2, v_3). This also gives rise to the $\varepsilon_2 - \varepsilon_3$ and $v_2 - v_3$ correlation plots as shown in Figs. 3(e) and (f). It is clear that the spectator binning allows us to access novel geometries in terms of $(\varepsilon_2, \varepsilon_3)$ pairs which are never accessible in centrality binning alone. Moreover, since the trends are quite different along spectator bins, they cannot be accessed even if one performs a narrower centrality binning. For $(20–25)\%$ and more peripheral bins, there is much smaller correlation along $L+R$ bins as compared to that along centrality bins, e.g. in case of the $(20–25)\%$ centrality bin while v_3 changes by only 10% for different $L+R$ bins, v_2 varies by around 130%. This will allow us to disentangle the effects of v_2 from v_3 on other observables, e.g. the non-linear mode couplings during the hydrodynamic expansion that result in correlations in $(v_2 - v_4)$ and $(v_2, v_3 - v_5)$ could be studied. In this regard, it will be interesting to look at correlation plots of (v_2, v_4), (v_2, v_5) and (v_3, v_5) in data with a combined binning in $dN_{ch}/d\eta$ and $L+R$ bins. Thus, a combined binning in terms of centrality and $L+R$ allows us to disentangle the contribution of different IS characteristics on the FS observables. Here

we have discussed two such cases, (a) N_{part} and N_{coll} and their contribution towards FS $dN_{ch}/d\eta$ and (b) ε_2 and ε_3 and their contribution towards v_2 and v_3 respectively. In Fig. 4 we show the correlation between $N_{\mathrm{coll}}/N_{\mathrm{part}}$ with ε_2 and ε_3. Thus with the introduction of $L+R$ bins, we can now study the evolution of similar initial geometry $(\varepsilon_2, \varepsilon_3)$ but with different mechanism of energy deposition $(N_{\mathrm{coll}}/N_{\mathrm{part}})$.

Thus studies with $L+R$ bins can complement ongoing studies with q_2 bins which also aim at studying the influence of the event shape on various FS observables [22,23] where q_2 is obtained from the second harmonic flow vector Q_2 [21,22]

$$Q_2 = \sqrt{Q_{2,x}^2 + Q_{2,y}^2}, \quad q_2 = \frac{1}{\sqrt{M}} Q_2 \qquad (8)$$

Here $Q_{2,x}$ and $Q_{2,y}$ are computed using particles produced in the FS. It is important to note that unlike the q_2 binning procedure, in this method of studying the IS geometry through $L+R$ bins the linearity relationship between (v_2, v_3) and $(\varepsilon_2, \varepsilon_3)$ is not essential as the spectators, being IS observables, provide a direct access to the IS geometry.

Ideal fluid hydrodynamics is scale invariant and as a result the final value of the ratio (v_2/ε_2) attained is independent of the system size [24]. Viscous corrections in a non-ideal fluid arising due to incomplete thermalization introduce system size depen-
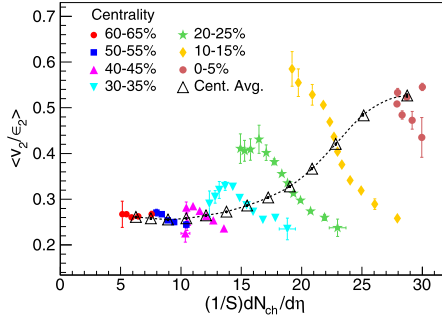
Fig. 5. (Colour online.) v_2/ε_2 vs $(1/S)\,dN_{ch}/d\eta$ for different centrality and $L+R$ bins. The $L+R$ bins break the scaling relation between v_2/ε_2 and $(1/S)\,dN_{ch}/d\eta$ that is exhibited by centrality bins.

dence and tend to reduce this ratio. The ratio of the microscopic mean free path λ to the typical macroscopic system size Λ, λ/Λ is called the Knudsen number K. K^{-1} is expected to be a good measure of the thermalization achieved [24,1]. Since v_2 develops over some time during which the fireball rapidly expands it is not exactly clear what should be the value of λ and Λ to be used to determine the degree of thermalization. In earlier studies, it has been suggested that v_2 dominantly develops in the early stage of the fireball evolution. Therefore K^{-1} estimated at time $\tau \sim \Lambda_T/c_s$ at the onset of transverse expansion of the fireball, should be used as a measure of thermalization [24,1]. Here Λ_T is the transversize size of the fireball on the collision plane and c_s is the speed of sound. It was further argued that K^{-1} at Λ_T/c_s approximately scales with $(1/S)\,dN_{ch}/d\eta$ where S is the initial transverse area on the collision plane. Similar scaling relation between v_2/ε_2 and $(1/S)\,dN_{ch}/d\eta$ is also expected in the low density regime [25–27]. Previous analysis of experimental data with centrality binning have indeed found very good scaling relation between v_2/ε_2 vs $(1/S)\,dN_{ch}/d\eta$ for different systems like Cu + Cu and Au + Au [1,4]. The detailed mechanism of energy deposition in the initial stages of a HIC event which ultimately leads to particle production is yet to be understood completely. With centrality as the only tuning parameter to separate different initial conditions, it is difficult to discriminate between predictions from models with different mechanisms of particle production. Now, with the introduction of $L+R$ bins, we are able to pin down the initial conditions more precisely. In Fig. 5 we have plotted the ratio v_2/ε_2 vs $(1/S)\,dN_{ch}/d\eta$ with centrality and $L+R$ bins. The centrality averaged points exhibit the usual trend of an initial fast rise and final saturation of the ratio v_2/ε_2 with $(1/S)\,dN_{ch}/d\eta$. However, the $L+R$ bins in each centrality show the opposite behaviour and breaks the usual scaling relation. In a given centrality bin, with rise in $L+R$, the transverse overlap area S sharply falls while $dN_{ch}/d\eta$ is almost constant. Thus $(1/S)\,dN_{ch}/d\eta$ which acts like a proxy for K^{-1} increases with $L+R$ although the hydrodynamic

response v_2/ε_2 falls sharply. As mentioned earlier, we expect more (less) hot spots and gradients in the initial energy profile of events with larger (smaller) $L+R$ leading to more (less) viscous correction. This ultimately leads to inefficient conversion of the initial ε_n to the final v_n in events with larger $L+R$ as compared to those with smaller $L+R$.

The ratio v_n/ε_n is also expected to exhibit acoustic scaling and receives viscous corrections that grow exponentially as n^2 and $1/\Lambda_T$ [28–31]

$$\ln\left(\frac{v_n}{\varepsilon_n}\right) \propto -\frac{4}{3}\frac{n^2\eta}{\Lambda_T Ts}, \tag{9}$$

with the typical initial transverse size of the system Λ_T given by $1/\Lambda_T = \sqrt{1/\sigma_x^2 + 1/\sigma_y^2}$. Such acoustic scaling was found in data across a wide range of beam energies and the shear viscosity to entropy density ratio, η/s was extracted from the slope of the plot, $\ln\left(\frac{v_2}{\varepsilon_2}\right)$ vs $1/\Lambda_T$ [29–31]. These studies were done with centrality binning alone. Here we perform a consistency check of such scaling laws using simulated data by including $L+R$ bins in every centrality bin. In Figs. 6(a) and (b) we have plotted $\ln(v_2/\varepsilon_2)$ and $\ln(v_3/\varepsilon_3)$ respectively vs $1/\Lambda_T$. We find approximate simulated data collapse for $(0-40)\%$ centrality as well as their corresponding $L+R$ bins. On a closer scrutiny, it seems that the slope parameter for bins of different $L+R$ but a particular centrality is different from those of a different centrality resulting in a mild breaking of the acoustic scaling. Thus, the introduction of the $L+R$ bins enable a more refined extraction of η/s from data.

So far we have discussed results for events first binned by dN_{ch}/dy followed by $L+R$. If b was the only E/E fluctuating quantity, then b, dN_{ch}/dy and $L+R$ would have a one to one correspondence and hence the final results would be independent of the order of the binning procedure. However, as discussed earlier, in HICs there are additional sources of E/E fluctuations apart from the geometrical fluctuation in b. This means that the final results are sensitive to the order of the binning procedure. In order to illustrate this point we have also analysed the events in the reverse binning procedure: first we bin by $L+R$ followed by dN_{ch}/dy. We have shown a few results in Figs. 7 and 8. As seen from Fig. 7(a), σ_x which is also a measure of the initial system size is almost constant in a particular $L+R$ bin even though N_{part} changes resulting in the strong variation of N_{coll}/N_{part} within a $L+R$ bin as shown in Fig. 7(b). This finally translates into a stronger variation in $dN_{ch}/d\eta$ within a $L+R$ bin with N_{part} as compared to the variation between different $L+R$ bins. This further results in the trends between v_2/ε_2 and $1/SdN_{ch}/dy$ as seen in Fig. 8(a). Within a particular $L+R$ bin, the bins with higher $1/SdN_{ch}/dy$ have higher N_{coll}/N_{part} ratio than the average trend resulting in smaller v_2/ε_2 compared to the average trend. This trend was seen even in the earlier binning procedure. As seen in Fig. 8(b), the acoustic scaling
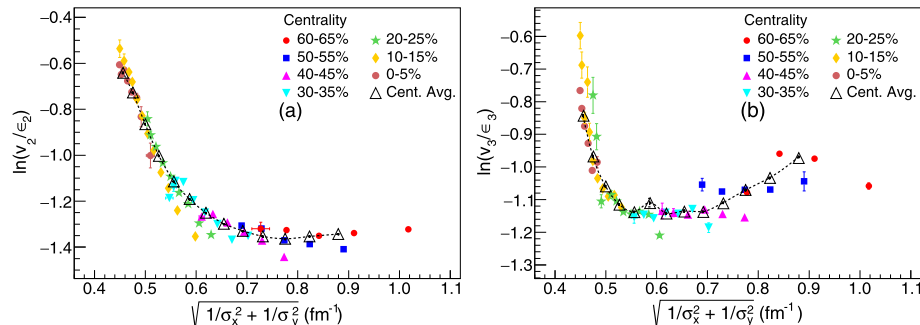

Fig. 6. (Colour online.) Acoustic scaling of the hydrodynamic response $\ln(v_n/\varepsilon_n)$ vs $1/\Lambda_T$ with $n=2$ (left) and $n=3$ (right) for different centrality and $L+R$ bins.
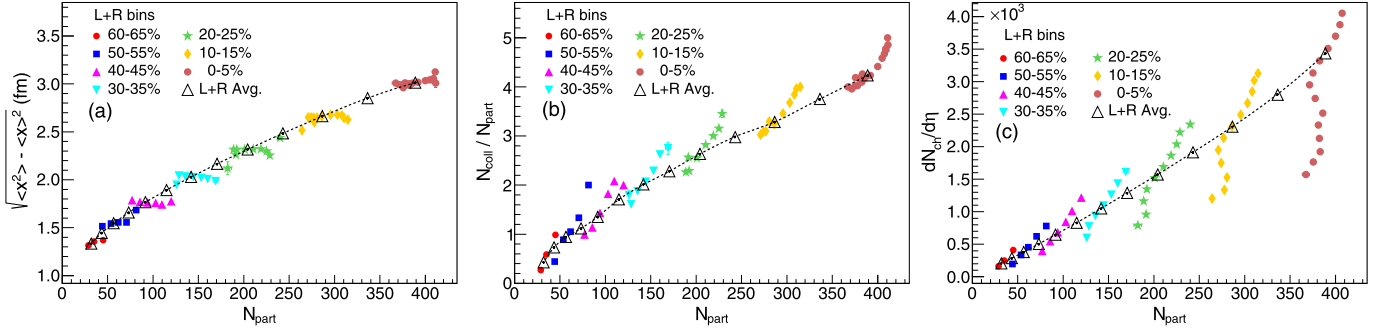
Fig. 7. (Colour online.) Different qualitative dependence of σ_x, N_{coll} and $dN_{ch}/d\eta$ on N_{part} with the reverse binning procedure (first binned by $L + R$ followed by $dN_{ch}/d\eta$) are shown.
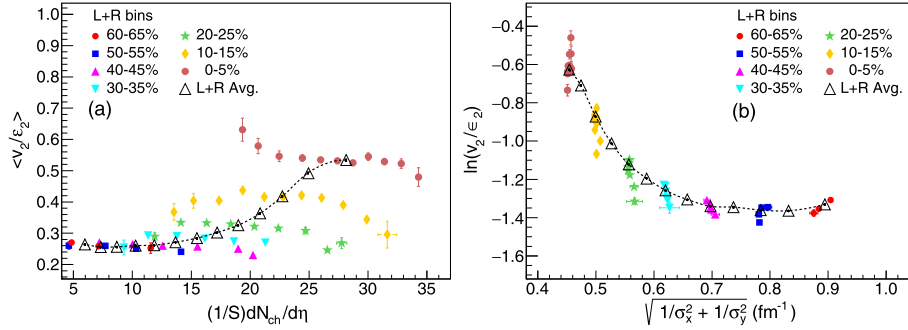

Fig. 8. (Colour online.) v_2/ε_2 vs $(1/S) \, dN_{ch}/d\eta$ and $1/\Lambda_T$ with the reverse binning procedure (first binned by $L + R$ followed by $dN_{ch}/d\eta$) are shown.

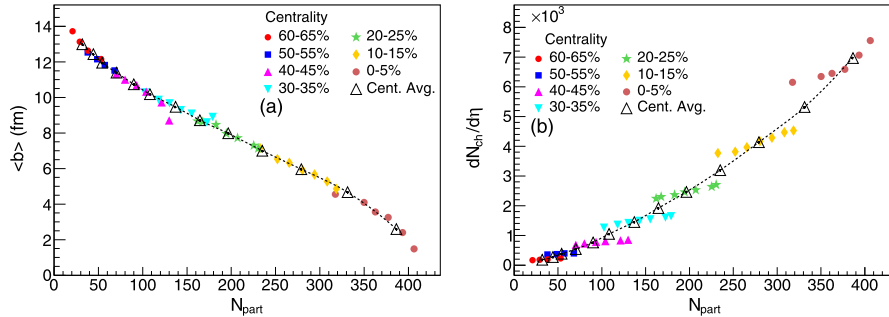**Fig. 9.** (Colour online.) The trends for $dN_{ch}/d\eta$ and b with N_{part} as obtained in HIJING where the events were binned by $dN_{ch}/d\eta$ followed by $L + R$.

relation as in Eqn. (9) does not hold anymore as the slope for the trend of the average $L + R$ bins is much softer than the slope along different dN_{ch}/dy bins in the same $L + R$ bin. Thus this breaking of the acoustic scaling relation which was mild in the earlier binning procedure becomes much stronger in the reverse binning procedure.

So far all our results have been from the AMPT model. We will now show a few results for the combined binning procedure with dN_{ch}/dy followed by $L + R$ in HIJING event generator. In Figs. 9(a) and (b) we show the results for b and dN_{ch}/dy and find them to be very similar to what we obtain in the case of AMPT in Figs. 1(c) and 2(d). AMPT takes into account later stage interactions in the partonic as well as hadronic phases while in HIJING such interactions are absent. As seen in Fig. 10, this results in very different trends for $\langle p_T \rangle$ with N_{part} in AMPT compared to HIJING. In AMPT, we find the $\langle p_T \rangle$ trends along $L + R$ bins to be much different to that of the average trend along different centrality bins with $\sim$10–15% variation in a particular $dN_{ch}/d\eta$ bin for different $L + R$ bins. On the other hand, in HIJING the $\langle p_T \rangle$ trends do not depend on the binning procedure and is a single-valued with N_{part}. We conclude that this starkly different trends of $\langle p_T \rangle$ in the two cases

should be stemming from the fact that medium effects which are taken into account in AMPT are missing in HIJING. In the different $L + R$ bins there is different degree of medium interactions and collectivity resulting in different values of the final $\langle p_T \rangle$. Our earlier observation of different values of v_2/ε_2 along different $L + R$ bins support the above conclusion as well. Thus measurement of $\langle p_T \rangle$ with such combined binning procedure can also throw light on the degree of collectivity achieved. We note from Fig. 5 that in a particular $dN_{ch}/d\eta$ bin, those $L + R$ bins which have the least v_2/ε_2 also have the highest $\langle p_T \rangle$ in Fig. 10(a).

4. Summary

We have demonstrated using the AMPT model the important role played by the spectators to determine the initial condition in heavy-ion collisions. The standard procedure involves binning events by their final state multiplicity. This however puts events with varying initial conditions into the same bin as long as they produce similar multiplicity. We demonstrate that by further binning events according to the total number of spectator neutrons, it is possible to separate events with different initial conditions
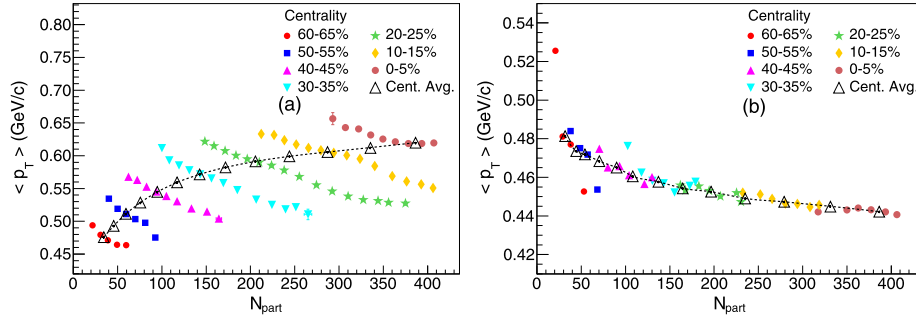
Fig. 10. (Colour online.) The trend for $\langle p_T \rangle$ with N_{part} as obtained in AMPT (a) and HIJING (b) where the events were binned by $dN_{ch}/d\eta$ followed by $L + R$.

which were earlier clubbed together in the same centrality bin. This new methodology provides an opportunity to study events with rare initial conditions. Moreover it is possible to vary ε_2 and ε_3 independently of each other. This enables one to extract the contribution due to non-linear mode coupling between v_2 and v_4 and (v_2, v_3) and v_5. It is important to note that for this purpose it is not essential to know $L + R$ very accurately. We found the variation of $dN_{ch}/d\eta$ with N_{part} to be much different for $L + R$ bins compared to usual centrality bins thus allowing us to study different energy deposition mechanism within the same centrality. We argued that in a given centrality bin, larger $L + R$ bins have higher energy gradients and more number of energy hot spots as compared to smaller $L + R$ bins which result in strong inhomogeneities in the initial conditions. This calls for larger viscosity driven effects and hence smaller v_2/ε_2 for bins with higher $L + R$. This also results in the breaking of the scaling relation between v_2/ε_2 and $\frac{1}{S} dN_{ch}/d\eta$ by the $L + R$ bins. A comparatively milder breaking of the acoustic scaling relation between $\ln(v_n/\varepsilon_n)$ and the initial system transverse size is observed for both centrality as well as $L + R$ bins. The results from this study suggest that one might be able to extract a more accurate value of the η/s ratio with the introduction of the $L + R$ bins. We also observe that $\langle p_T \rangle$ in combined bins of $dN_{ch}/d\eta$ and $L + R$ is a good probe to measure the degree of medium interaction and again in this case a precise measurement of $L + R$ is not necessary. Hence even with the current performance of the ZDCs, we should be able to perform some of these analysis in data.

References

[1] H.-J. Drescher, A. Dumitru, C. Gombeaud, J.-Y. Ollitrault, Phys. Rev. C 76 (2007) 024905, arXiv:0704.3553 [nucl-th].
[2] P. Romatschke, U. Romatschke, Phys. Rev. Lett. 99 (2007) 172301, arXiv:0706.1522 [nucl-th].
[3] M. Luzum, P. Romatschke, Phys. Rev. C 78 (2008) 034915, arXiv:0804.4015 [nucl-th];
M. Luzum, P. Romatschke, Phys. Rev. C 79 (2009) 039903 (Erratum).
[4] H. Song, S.A. Bass, U. Heinz, T. Hirano, C. Shen, Phys. Rev. Lett. 106 (2011) 192301, arXiv:1011.2783 [nucl-th];
H. Song, S.A. Bass, U. Heinz, T. Hirano, C. Shen, Phys. Rev. Lett. 109 (2012) 139904 (Erratum).
[5] V. Roy, A.K. Chaudhuri, B. Mohanty, Phys. Rev. C 86 (2012) 014902, arXiv:1204.2347 [nucl-th].
[6] V. Roy, B. Mohanty, A.K. Chaudhuri, J. Phys. G 40 (2013) 065103, arXiv:1210.1700 [nucl-th].
[7] S. Chatterjee, P. Tribedy, Phys. Rev. C 92 (2015) 011902, arXiv:1412.5103 [nucl-th].
[8] V. Bairathi, M.R. Haque, B. Mohanty, Phys. Rev. C 91 (2015) 054903, arXiv:1504.04719 [nucl-ex].
[9] J. Jia, S. Radhakrishnan, M. Zhou, arXiv:1506.03496 [nucl-th], 2015.
[10] B. Abelev, et al., ALICE Collaboration, Phys. Rev. C 88 (2013) 044909, arXiv:1301.4361 [nucl-ex].
[11] S. Tarafdar, Z. Citron, A. Milov, Nucl. Instrum. Methods A 768 (2014) 170, arXiv:1405.4555 [nucl-ex].
[12] Z.-w. Lin, C. Ko, Phys. Rev. C 65 (2002) 034904, arXiv:nucl-th/0108039.
[13] Z.-W. Lin, C.M. Ko, B.-A. Li, B. Zhang, S. Pal, Phys. Rev. C 72 (2005) 064901, arXiv:nucl-th/0411110.
[14] X.-N. Wang, M. Gyulassy, Phys. Rev. D 44 (1991) 3501.
[15] B. Zhang, Comput. Phys. Commun. 109 (1998) 193, arXiv:nucl-th/9709009.
[16] B. Andersson, G. Gustafson, G. Ingelman, T. Sjostrand, Phys. Rep. 97 (1983) 31.
[17] R.S. Bhalerao, J.-Y. Ollitrault, Phys. Lett. B 641 (2006) 260, arXiv:nucl-th/0607009.
[18] A. Bialas, M. Bleszynski, W. Czyz, Nucl. Phys. B 111 (1976) 461.
[19] X.-N. Wang, M. Gyulassy, Phys. Rev. Lett. 86 (2001) 3496, arXiv:nucl-th/0008014.
[20] D. Kharzeev, M. Nardi, Phys. Lett. B 507 (2001) 121, arXiv:nucl-th/0012025.
[21] A.M. Poskanzer, S.A. Voloshin, Phys. Rev. C 58 (1998) 1671, arXiv:nucl-ex/9805001.
[22] J. Schukraft, A. Timmins, S.A. Voloshin, Phys. Lett. B 719 (2013) 394, arXiv:1208.4563 [nucl-ex].
[23] P. Huo, J. Jia, S. Mohapatra, Phys. Rev. C 90 (2014) 024910, arXiv:1311.7091 [nucl-ex].
[24] R.S. Bhalerao, J.-P. Blaizot, N. Borghini, J.-Y. Ollitrault, Phys. Lett. B 627 (2005) 49, arXiv:nucl-th/0508009.
[25] H. Heiselberg, A.-M. Levy, Phys. Rev. C 59 (1999) 2716, arXiv:nucl-th/9812034.
[26] S.A. Voloshin, A.M. Poskanzer, Phys. Lett. B 474 (2000) 27, arXiv:nucl-th/9906075.
[27] P.F. Kolb, P. Huovinen, U.W. Heinz, H. Heiselberg, Phys. Lett. B 500 (2001) 232, arXiv:hep-ph/0012137.
[28] P. Staig, E. Shuryak, Phys. Rev. C 84 (2011) 034908, arXiv:1008.3139 [nucl-th].
[29] R.A. Lacey, A. Taranenko, N.N. Ajitanand, J.M. Alexander, arXiv:1105.3782 [nucl-ex], 2011.
[30] R.A. Lacey, Y. Gu, X. Gong, D. Reynolds, N. Ajitanand, et al., arXiv:1301.0165, 2013.
[31] R.A. Lacey, A. Taranenko, J. Jia, D. Reynolds, N. Ajitanand, et al., Phys. Rev. Lett. 112 (2014) 082302, arXiv:1305.3341 [nucl-ex].